
Article:
Wu, Xiugang, Xie, Guohua, Cabry, Christopher P. et al. (6 more authors) (2018) Linearly polarized electroluminescence from ionic iridium complex-based metallomesogens : The effect of aliphatic-chain on their photophysical properties. Journal of Materials Chemistry C. pp. 3298-3309. ISSN 2050-7534

https://doi.org/10.1039/c7tc05421a

Linearly Polarized Electroluminescence from Ionic Iridium Complex-based Metallomesogens: The Effect of Aliphatic-Chain on Their Photophysical Properties

Xiugang Wu,† Guohua Xie,‖ Christopher P. Cabry,& Xiaoyu Xu,‡ Stephen J. Cowling,& Duncan W. Bruce,&* Weiguo Zhu,‡ Etienne Baranoff‡*, Yafei Wang,†*

† *Jiangsu Key Laboratory of Environmentally Friendly Polymeric Materials, School of Materials Science & Engineering, Changzhou University, Changzhou 213164, PR China*

‡ *School of Chemistry, University of Birmingham, Birmingham B15 2TT, UK*

& *Department of Chemistry, University of York, Heslington, York*, *YO10 5DD*.

‖ *Department of Chemistry, Hubei Key Lab on Organic and Polymeric Optoelectronic Materials, Wuhan University, Wuhan 430072, People's Republic of China.*

Corresponding author

Yafei Wang: qiji830404@hotmail.com

Duncan W. Bruce: duncan.bruce@york.ac.uk

Etienne Baranoff: eb.chimie@gmail.com

Abstract

Directly polarized organic light emitting diodes (OLEDs) have the potential to significantly improve the efficiency and reduce the cost of liquid-crystal displays (LCDs) among other applications. However, fluorescent liquid crystals are currently used to achieve this, while phosphorescent emitters would further improve efficiency. To this end, the metallomesogens based on ionic iridium complexes bearing different aliphatic chains substituent, named **7a** and **7b**, were designed and prepared in this contribution. Both iridium complexes showed smectic mesophase evidenced by differential scanning calorimetry, polarized optical microscopy and X-ray diffraction. Deep-red emission was observed for the iridium complexes in solution and solid state, and complex **7a** clearly presented aggregation-induced emission (AIE) behavior in THF-water solvent mixture. Non-doped polarized OLEDs employing complex **7a** or **7b** as emitter were fabricated and direct linearly polarized electroluminescence with a polarization ratio of 4 was achieved, which is the highest ratio reported for metallomesogens-based phosphorescent OLEDs. Importantly, the choice of linker between the core complex and mesogenic pendent groups is key to achieve distinctive polarization of electroluminescence and AIE. These results are a first step towards the development phosphorescent OLEDs able to efficiently produce polarized electroluminescence.

Keywords

Metallomesogens; Iridium complex; Deep-red emission; Aggregation-induced emission; Polarized electroluminescence

Introduction

Since the demonstration of linearly polarized electroluminescence (EL) from an oriented polymer by Dyreklev *et al.*,[1] luminescent liquid crystals have attracted increased attention for applications in organic light-emitting diodes (OLEDs).[2-4] The main incentive is the promise of polarizer-free devices, which would improve the efficiency and reduce the cost of backlights for liquid crystal displays (LCDs).

In order to realize polarized EL, numerous efforts have been devoted to the preparation of luminescent liquid crystals based on fluorescent small molecules, oligomers and polymers by combining flexible aliphatic chains with rigid photoactive units, in particular fluorene.[5-11] While the full range of colors, including white, and high polarization ratio >30 are obtained with such materials, the intrinsic singlet-only harvesting ability of fluorescent materials is an important limitation for the development of highly efficient polarized OLEDs.

Phosphorescent OLEDs can be significantly more efficient than fluorescent OLEDs due to the ability to harvest both singlet and triplet excitons.[12,13] Hence the introduction of heavy metals into liquid-crystalline materials (phosphorescent metallomesogens) is a promising strategy to develop highly efficient polarized OLEDs. Platinum complexes are particularly attractive candidates because of their favorable phosphorescence properties that favor high efficiency EL[14-23] and the square-planar geometry that favor the formation of liquid crystalline materials.[24-32] Liu *et al.* have reported linearly polarized EL based on a liquid-crystalline platinum complex doped into an oligofluorene matrix.[33,34] The device displayed current efficiency up to 2.4 cd A^{-1} with

maximum luminance exceeding 2000 cd m^{-2} but with a polarization ratio of only ~2. However, the square-planar structure of platinum complex is often liable to formation of aggregates, which and lead to aggregation-caused quenching of emission in concentrated solution and neat film. Therefore, phosphorescent liquid crystal material with intense emission in concentrated state is an ongoing challenge.

The most common strategy to increase emission intensity in concentrated state is to graft bulky groups onto the emissive core to reduce detrimental intermolecular interactions.[35,36] To favor the formation of LC phases, pro-mesogenic fragments/or flexible chains are used as sterically hindering moieties[37-39] and, for example, successfully generated liquid crystals based on non-mesogenic cores such as fullerene and metal cluster.[40,41] However, few these liquid crystalline with steric structure showed a satisfied emissive property in the visible light region. Cyclometalated iridium complexes, , widely used as highly efficient OLEDs emitters but with an octahedral structure unfavorable to the formation of LC phases, can also benefit from the same approach to devise efficient phosphorescent metallomesogens. .[42-45] Yet, such cyclometalated iridium complexes have never been used for directly polarized EL. This is attributed to their quasi-spherical structure impeding the anisotropic alignment of transition dipole moments necessary for polarized emission.

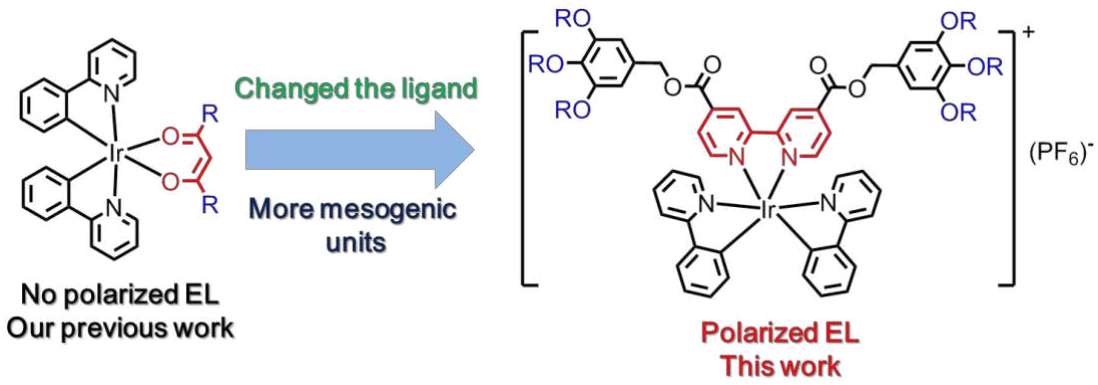

Chart 1. Structural evolutions of iridium complex based metallomesogens

In our ongoing efforts to the investigate iridium complex-based metallomesogens to achieve polarized EL, we prepared two new ionic, liquid-crystalline iridium complexes (**7a**/**7b** in Scheme 1) by grafting highly mesogenic 2,3-difluoro-4'-(4-pentylcyclohexyl)biphenyl moieties onto a bipyridine ancillary ligand. Compared to our previous work (Chart 1),[45] herein we introduced additional mesogenic units onto the iridium core to enhance its organization in the neat film. To investigate the structure-property of two phosphorescent metallomesogens, different linkers between the core complex and the mesogenic groups were designed. In complex **7a**, the linker between the core complex and the mesogenic groups is a lipophilic hexyl chain, while in **7b** the linker is a hydrophilic triethyleneglycol chain. Both cyclometalated iridium complexes based metallomesogens presented distinct photophysical properties. Complex **7a** rather than **7b** showed a clearly AIE property in THF/H_2O mixture. Identically, the modification of linkers has a tremendous impact on their ability to display polarized EL.

Experimental Section

General information

All reagents were purchased from Aldrich and VWR and used as received. Compounds **1**, **2**, **4a**, and **5a** were synthesized as previously reported.[39,45] All reactions and manipulations were carried out under Ar atmosphere with the use of standard inert atmosphere techniques. ^{1}H NMR spectra were measured in $CDCl_3$ solution on a Bruker DPX (300 MHz and 400 MHz) NMR spectrometer with tetramethylsilane (TMS) as the internal standard. Mass spectra (MS) were recorded on a Bruker Autoflex TOF/TOF (MALDI-TOF) instrument using dithranol as a matrix. UV-vis absorption spectroscopy was measured by Shimadzu UV-265 spectrometer at room temperature. Luminescence spectra were recorded on RF-5301 PC (Perkin Elmer) at room temperature in dichloromethane (10^{-5} M, uncorrected spectra). Birefringence phenomenon was observed and recorded by polarizing optical microscope (POM, Olympus, BH-2), with a hot stage (Mettler, FP80HT) and controller (Mettler, FP80HT). Differential scanning calorimetry (DSC) was carried out to evaluate the phase transition temperatures and enthalpies of iridium complexes using a DSC Q10 calorimeter under N_2 atmosphere with heating and cooling rate 10 ^{o}C/min. Thermal gravimetric analysis (TGA) was carried out using a TQAQ-50 instrument with heating rate as 20 ^{o}C/min under N_2 atmosphere. X-ray diffraction was measured by Bruker D8 Discover diffractometer with a 2D Vantec detector. Sample is mounted in a capillary in a bespoke heating environment-a hollow graphite furnace-with temperature control via an Eurotherm controller.

Procedure for SEM sample

Scanning electron microscopy (SEM) images were recorded using JEOL-7000 SEM instruments. As for the SEM sample, we firstly cleared the substrate which is the copper sheet. Secondly, the THF/H_2O mixture solution was dropped upon the copper sheet. After the solution volatilized at room temperature, the sample was then dried by the vacuum pump at room temperature.

Devices fabrication and characterization

A layer of poly(3,4-ethylenedioxythiophene): poly(styrenesulfonate) (PEDOT:PSS) was spin-coated on the ITO glass substrate after UV-ozone treatment. After baking of PEDOT:PSS at 120 °C for 10 min, another layer of poly(N-vinylcarbazole) (PVK) was spin-coated directly and then baked at 120 °C for another 10 min. In order to obtain polarized emission, we treated the emitting layer via different methods (see below) after spin-coating of the complexes onto the hole transporting layer PVK. An electron transporting layer of bis-4,6-(3,5-di-3-pyridylphenyl)-2-methylpyrimidine (B3PYMPM) was thermally evaporated on the emitting layer. All the devices were encapsulated under a nitrogen atmosphere using UV curable epoxy. The current-voltage-luminance characteristics were collected with a PR735 Spectrascan spectrometer and a Keithley 2400 programmable source meter. The (polarized) EL spectra were recorded by an Ocean Optics USB2000 spectrometer. The EL intensities parallel and perpendicular to the rubbing direction (along the ITO stripe) could be distinguished by aligning a linear polarizer inserted between the OLEDs and the spectrometer at two mutually perpendicular directions which were denoted as Hor and Ver.

To further explore the effect of alignment on the polarized emission, different alignment methods were tested for the active layer:(1) After spin-coating the iridium complex onto PVK layer, the emissive layer was heating to liquid crystalline state and then annealing for 30 min (7a: 225^{o}C; 7b: 160^{o}C, the same below). The devices configurations are: **Device I**: ITO/PEDOT:PSS(30 nm)/PVK(30 nm)/iridium complex (50 nm)/Ca(100nm) /Al(100 nm). **Device II**: ITO/PEDOT:PSS(30 nm)/PVK(30 nm)/iridium complex (50 nm)/B3YMPM(50 nm)/Ca(100 nm)/Al(100 nm). Compared to **Device I**, **Device II** has an additional electron transporting layer. (2) In this procedure, the hole transporting layer of PVK was used as the alignment layer. The PVK was rubbed (at 120^{o}C) with a dustless cloth for its surface alignment in one direction (the fabrication procedure for PVK is above). Then, the iridium complex was spin-coated onto PVK layer. The iridium complex was heated to liquid crystalline state and annealing. The device configuration is: **Device III**: ITO/PEDOT:PSS(30 nm)/PVK(30 nm, rubbed)/iridium complex (50 nm)/B3YMPM(50 nm)/ Ca(100 nm)/Al(100 nm). (3) In this method, the iridium complexes were heated to liquid crystal state and then directly rubbed with the dustless cloth after they were spin-coated onto PVK layer. Then the iridium complex was annealing (the temperature is same with above). The device configuration is: **Device IV**: ITO/PEDOT:PSS(30 nm)/PVK(30 nm)/iridium complex (50 nm, rubbed)/B3YMPM(50 nm)/ Ca(100 nm)/Al(100 nm)

Synthesis of 2

A mixture of **1** (3.0 g, 8.4 mmol), 1,2-bis(2-(*p*-tosyloxy)ethoxy)ethane (3.8 g, 8.4 mmol), K_2CO_3 (1.7 g, 12.6 mmol), KI (0.13 g, 0.8 mmol) and acetonitrile (60 mL) was

refluxed under argon for 24 hours. After cooling to room temperature, the solvent was removed under reduced pressure and the residue was purified by silica gel column chromatography (hexane/ethyl acetate = 20 :1) to obtain **2** as a white solid (3.9 g, 72 %). ^{1}H NMR ($CDCl_3$ 300 MHz): δ 7.80 (d, *J* = 8.4 Hz, 2H), 7.42 (dd, *J* = 8.4 Hz, 1.8 Hz, 2H), 7.34-7.26 (m, 2H), 7.09 (td, *J* = 8.7 Hz, 2.1 Hz, 1H), 6.84-6.78 (m, 1H), 4.19 (dt, *J* = 15.3 Hz, 4.5 Hz, 4H), 3.87 (t, *J* = 4.8 Hz, 2.1 Hz, 2H), 3.73-3.67 (m, 4H), 3.64-3.61 (m, 2H), 2.55-2.43 (m, 4H), 1.91 (t, *J* = 11.1 Hz, 4H), 1.46-1.04 (m, 13H), 0.90 (t, *J* = 6.9 Hz, 3H). ^{13}C NMR (100 MHz, $CDCl_3$): 152.0, 149.8, 147.2, 146.9, 144.5, 142.9, 132.7, 131.9, 129.5, 128.3, 127.6, 126.7, 123.2, 109.7, 70.6, 69.3, 68.9, 68.4, 44.0, 37.0, 37.0, 34.0, 33.2, 31.9, 26.3, 22.4, 21.3, 13.8.

Synthesis of 4b

A mixture of ethyl 3,4,5-trihydroxybenzoate (0.28 g, 1.4 mmol), **2** (3.5 g, 5.4 mmol) and K_2CO_3 (1.9 g, 14.0 mmol) in acetone was refluxed for 30 h under Ar. After cooling to RT, the reaction mixture was poured into water and extracted with CH_2Cl_2. The organic layer was washed with water, dried over $MgSO_4$ and removed by evaporator. The residue was purified by column chromatography on silica (Hexane/CH_2Cl_2 = 3:1) to give compound **4b** as a colorless oil (1.4 g, 63 %). ^{1}H NMR (300 MHz, $CDCl_3$): δ 7.42-7.38 (m, 6H), 7.29-7.24 (m, 8H), 7.05 (tt, *J* = 16.8 Hz, 8.7 Hz, 2.4Hz, 3H), 6.81-6.75 (m, 3H), 4.32 (q, *J* = 7.2 Hz, 2H), 4.25-4.18 (m, 12H), 3.99-3.82 (m, 12H), 3.75 (s, 12H), 2.49 (tt, *J* = 23.4 Hz, 12.0 Hz, 2.7Hz, 3H), 1.90 (t, *J* = 10.5 Hz, 12H), 1.49-1.03 (m, 42H), 0.90 (t, *J* = 6.6 Hz, 9H). ^{13}C NMR (100 MHz, $CDCl_3$): δ 166.1, 152.3, 147.4, 147.2, 142.5, 132.2, 128.6, 127.0, 125.3, 123.5, 109.9, 109.0, 72.4, 71.0, 70.6,

69.6, 68.9, 61.0, 44.3, 37.4, 37.3, 34.3, 33.6, 32.2, 26.7, 22.7, 14.1.

Synthesis of 5b

$LiAlH_4$ (1.24 mmol, 47 mg) was slowly added to a solution of **4b** (1.0 g, 0.62 mmol) in dry THF at 0 ^oC. The reaction mixture was stirred for 24 h at RT. A saturated NH_4Cl aqueous solution was slowly added at 0 ^oC to quench the reaction. The mixture was acidified with HCl (10%) to pH = 2. The aqueous phase was separated and extracted with CH_2Cl_2. The combined organic layers were washed with water, dried over $MgSO_4$ and solvents removed under reduced pressure. The residue was purified by column chromatography on silica gel (CH_2Cl_2) to give **5b** as a white solid (0.85 g, 87%). ^1H NMR (300 MHz, $CDCl_3$): δ 7.40 (dd, *J* = 8.1 Hz, 1.5 Hz, 6H), 7.27-7.24 (m, 6H), 7.08-7.01 (m, 3H), 6.812-6.75 (m, 3H), 6.60 (s, 2H), 4.54 (s, 2H), 4.22-4.14 (m, 12H), 3.89-3.81 (m, 12H), 3.74 (s, 12H), 2.49 (t, *J* = 12.3 Hz, 3H), 1.89 (*J* = 10.8 Hz, 12H), 1.49-1.03 (m, 39H), 0.89 (t, *J* = 6.6 Hz, 9H). ^{13}C NMR (100 MHz, $CDCl_3$): 152.8, 150.0, 147.5, 143.6, 140.8, 137.8, 136.6, 132.3, 128.7, 127.1, 123.6, 110.1, 109.4, 106.4, 72.4, 71.1, 70.6, 69.9, 69.6, 68.9, 65.4, 44.4, 37.5, 37.4, 34.4, 33.7, 32.3, 26.7, 22.8, 14.2.

Synthesis of 6a/6b

2,2'-Bipyridine-4,4'-dicarboxylic acid was refluxed overnight with an excess of thionyl chloride. The volatiles were removed under vacuum and the reaction mixture dried thoroughly under vacuum and used for next step without any further purification. 2,2'-bipyridine-4,4'-dicarbonyl dichloride (1 eq.) was dissolved in dry CH_2Cl_2 and added dropwise to a stirred solution of **5a**/**5b**(2.1 eq.) and triethylamine (3 mL) in dry CH_2Cl_2. The reaction mixture was refluxed for 12 h. The volatiles were removed under reduced

pressure and the reaction mixture purified with flash silica gel chromatography (CH_2Cl_2/CH_3OH = 100:1) to yield a white solid.

6a: white solid (1.2 g), yield: 52%. ^{1}H NMR (300 MHz, $CDCl_3$): δ 8.98 (s, 2H), 8.83 (d, *J* = 5.1 Hz, 2H), 7.91 (dd, *J* = 4.8 Hz, 1.5 Hz, 2H), 7.41-7.37 (m, 12H), 7.25-7.22 (m, 12H), 7.07-6.99 (m, 6H), 6.76-6.70 (m, 6H), 6.67 (s, 4H), 5.31 (s, 4H), 4.06-3.98 (m, 24H), 2.48 (t, *J* = 12.3 Hz, 6H), 1.93-1.85 (m 52H), 1.49-1.03 (m, 98H), 0.90 (t, *J* = 6.9 Hz, 18H). ^{13}C NMR (100 MHz, $CDCl_3$): δ 165.0 (O=C), 156.48 (bipyridine, C-2,2'), 153.18 (bipyridine, C-6,6'), 150.08 (bipyridine, C-4,4'), 147.36 (Ar-C), 142.90 (Ar-C), 140.40 (Ar-C), 138.70 (Ar-C), 138.33 (Ar-C), 132.30 (Ar-C), 132.29 (Ar-C), 130.39 (Ar-C), 128.55 (Ar-C), 127.0 (Ar-C), 123.48 (Ar-C), 122.96 (Ar-C), 120.64 (Ar-C), 114.69 (Ar-C), 109.46 (Ar-C), 107.35 (Ar-C), 73.21 (-Ar-CH_2O-), 69.66 (-CH_2O-), 68.95 (-CH_2O-), 44.32 (-CH_2-), 37.38 (-CH_2-), 34.28 (-CH_2-), 33.57 (-CH_2-), 32.22 (-CH_2-), 30.21 (-CH_2-), 29.29 (-CH_2-), 26.65 (-CH_2-), 25.87 (-CH_2-), 22.71 (-CH_2-), 14.11 (-CH_3). MS (MALDI-TOF) *m/z*: calcd. for $C_{200}H_{248}F_{12}N_2O_{16}$: 3161.85; found, 3162.5 $[M+H]^+$.

6b: white solid (0.98 g), yield: 41%. ^{1}H NMR (300 MHz, $CDCl_3$): δ 8.96 (s, 2H), 8.82 (d, *J* = 4.8 Hz, 2H), 7.83 (dd, *J* = 5.1 Hz, 1.8 Hz, 2H), 7.40-7.38 (m, 12H), 7.26-7.23 (m, 12H), 7.04 (td, *J* = 8.7 Hz, 2.4 Hz, 6H), 6.79-6.73 (m, 6H), 6.70 (s, 4), 5.27 (s, 4H), 4.18 (q, *J* = 4.2 Hz, 24H), 3.86 (t, *J* = 4.8 Hz, 24H), 3.74 (s, 24H), 2.53-2.44 (m, 6H), 1.89 (t, *J* = 10.2 Hz, 14H), 1.60-1.29 (m, 74H), 1.1-0.99 (m, 14H), 0.90 (t, *J* = 6.6 Hz, 18H). ^{13}C NMR (100 MHz, $CDCl_3$): δ 152.8 (bipyridine, C-2,2'), 151.8 (bipyridine, C-6,6'), 150.1 (bipyridine, C-4,4'), 149.5 (Ar-C), 147.7 (Ar-C), 147.6 (Ar-C), 147.4 (Ar-

C), 147.2 (Ar-C), 132.2 (Ar-C), 130.7 (Ar-C), 128.6 (Ar-C), 127.0 (Ar-C), 123.5 (Ar-C), 120.6 (Ar-C), 113.3 (Ar-C), 109.9 (Ar-C), 108.3 (Ar-C), 104.4 (Ar-C), 72.4 (-Ar-CH_2O-), 71.0 (-OCH_2CH_2O-), 70.9 (-OCH_2CH_2O-), 70.6 (-OCH_2CH_2O-), 69.8 (-OCH_2CH_2O-), 69.5 (-OCH_2-), 69.0 (-OCH_2-), 44.3 (-CH_2-), 37.4 (-CH_2-), 34.3 (-CH_2-), 33.6 (-CH_2-), 32.2 (-CH_2-), 26.6 (-CH_2-), 22.7 (-CH_2-), 14.1 (-CH_3). MS (MALDI-TOF) *m/z*: calcd. for $C_{200}H_{248}F_{12}N_2O_{28}$: 3353.79; found, 3376.1 $[M+Na]^+$.

Synthesis of complexes 7a/7b

A mixture of 2-phenylpyridine and $IrCl_3$•H_2O in 2-ethoxylethanol and water (*V*/*V*=3:1) was stirred overnight at 100°C under N_2. After cooling to room temperature, the precipitate was collected by filtrating, and washed with water, hexane and methanol. A yellow solid was obtained and used to the next step without any further purification. **6a/6b** (1 eq.) and chloro bridged iridium dimer (2 eq.) were dissolved in CH_2Cl_2/MeOH (*V*/*V* 3:1) and the mixture was stirred at 40 °C overnight. After cooling to RT, KPF_6 (5 eq.) was added to the solution and the reaction mixture was stirred for another 4 h at RT. The solvents were removed under reduced pressure and the residue was purified with column chromatography on silica gel (CH_2Cl_2/CH_3OH = 100:1) to yield a red solid. **7a:** red solid (82 mg), Yield: 34%. ^{1}H NMR (300 MHz, $CDCl_3$): δ 9.04 (s, 2H), 8.07 (d, *J* = 5.7 Hz, 2H), 7.93 (d, *J* = 5.7 Hz, 2H), 7.83 (d, *J* = 11.1 Hz, 2H), 7.70-7.62 (m, 4H), 7.54 (d, *J* = 5.7 Hz, 2H), 7.42-7.37 (m, 12H), 7.26-7.22 (m, 12H), 7.07-6.99 (m, 10H), 6.92-6.87 (m, 2H), 6.77-6.70 (m, 10H), 6.24 (d, *J* = 7.5 Hz, 2H), 5.33 (s, 4H), 4.05-3.98 (m, 24H), 2.52-2.45 (m, 6H), 1.25-1.77 (m, 54H), 1.48-1.24 (m, 82H), 1.11-0.99 (m, 14H), 0.9 (t, *J* = 6.6 Hz, 18H). ^{13}C NMR (100 MHz, $CDCl_3$): δ 167.2 (O=C), 163.0

(bipyridine,C-2,2'), 156.2 (bipyridine,C-6,6'), 153.2 (phenylpyridine, C-2), 151.2 (phenylpyridine, C-6), 150.1 (bipyridine,C-4,4'), 149.2 (Ar-C), 147.6 (Ar-C), 147.4 (Ar-C), 143.3 (Ar-C), 142.9 (Ar-C), 141.8 (Ar-C), 140.4 (Ar-C), 138.3 (Ar-C), 132.3 (Ar-C), 131.6 (Ar-C), 130.9 (Ar-C), 129.7 (Ar-C), 128.6 (Ar-C), 128.0 (Ar-C), 127.3 (Ar-C), 127.0 (Ar-C), 126.5 (Ar-C), 124.7 (Ar-C), 123.8 (Ar-C), 123.5 (Ar-C), 123.0 (Ar-C), 119.5 (Ar-C), 109.5 (Ar-C), 107.9 (Ar-C), 73.2 (-Ar-CH_2O-), 69.7 (-OCH_2-), 69.0 (-OCH_2-), 44.3 (-CH_2-), 37.4 (-CH_2-), 34.3 (-CH_2-), 33.6 (-CH_2-), 32.2 (-CH_2-), 30.2 (-CH_2-), 29.2 (-CH_2-), 26.7 (-CH_2-), 25.8 (-CH_2-), 22.7 (-CH_2-), 14.1 (-CH_3). Anal. calcd for $C_{222}H_{264}F_{18}IrN_4O_{16}P$: calcd C, 69.99; H, 6.99; N, 1.47. Found: C, 70.12; H, 6.97; N, 1.63. MS (MALDI-TOF) m/z: calcd. for $C_{222}H_{264}F_{18}IrN_4O_{16}P$: 3807.9; found, 3661.3 [M-PF_6].

7b: red solid (97 mg), Yield: 27%. ^{1}H NMR (300 MHz, $CDCl_3$): δ 9.17 (s, 2H), 8.09 (d, *J* = 5.4 Hz, 2H), 7.92 (dd, *J* = 5.4 Hz, 1.2 Hz, 2H), 7.84 (d, *J* = 8.1 Hz, 2H), 7.76-7.69 (m, 2H), 7.63 (d, *J* = 7.2 Hz, 2H), 7.58 (d, *J* = 5.7 Hz, 2H), 7.39-7.35 (m, 12H), 7.25-7.22 (m, 12H), 7.09-7.05 (m, 10H), 6.89 (td, *J* = 7.5 Hz, 1.2 Hz, 2H), 6.80-6.72 (10H), 6.23 (d, *J* = 6.9 Hz, 2H), 5.31 (s, 4H), 4.18 (q, *J* = 4.8 Hz, 24H), 3.88-3.85 (m, 24H), 3.73 (s, 24H), 2.52-2.43 (m, 6H), 1.72 (br, 14H), 1.52-1.03 (m, 88H), 0.90 (t, *J* = 6.6 Hz, 18H). ^{13}C NMR (100 MHz, $CDCl_3$): δ 167.32 (O=C), 162.94 (bipyridine,C-2,2'), 156.30 (bipyridine,C-6,6'), 152.84 (phenylpyridine, C-2), 151.58 (phenylpyridine, C-4), 150.12 (bipyridine,C-4,4'), 149.19 (Ar-C), 147.54 (Ar-C), 147.34 (Ar-C), 143.34 (Ar-C), 143.0 (Ar-C), 140.68 (Ar-C), 140.54 (Ar-C), 140.16 (Ar-C), 138.96 (Ar-C), 138.57 (Ar-C), 132.25 (Ar-C), 131.69 (Ar-C), 131.03 (Ar-C), 130.06 (Ar-C), 128.64

(Ar-C), 127.11 (Ar-C), 124.88 (Ar-C), 124.06 (Ar-C), 123.62 (Ar-C), 123.38 (Ar-C), 123.16 (Ar-C), 119.75 (Ar-C), 110.0 (Ar-C), 109.03 (Ar-C), 72.41 (-Ar-CH_2O-), 71.04 (-OCH_2CH_2O-), 70.86 (-OCH_2CH_2O-), 70.58 (-OCH_2CH_2O-), 69.83 (-OCH_2CH_2O-), 69.57 (-OCH_2-), 69.12 (-OCH_2-), 44.40 (-CH_2-), 37.46 (-CH_2-), 34.37 (-CH_2-), 33.65 (-CH_2-), 32.30 (-CH_2-), 26.74 (-CH_2-), 22.80 (-CH_2-), 14.20 (-CH_3). Anal. calcd for $C_{222}H_{264}F_{18}IrN_4O_{28}P$: calcd C, 66.63; H, 6.65; N, 1.40. Found: C, 66.07; H, 6.44; N, 1.65. MS (MALDI-TOF) *m/z*: calcd. for $C_{222}H_{264}F_{18}IrN_4O_{28}P$: 3999.84; found, 3852.7 [M-PF_6].

Results and Discussion

Synthesis

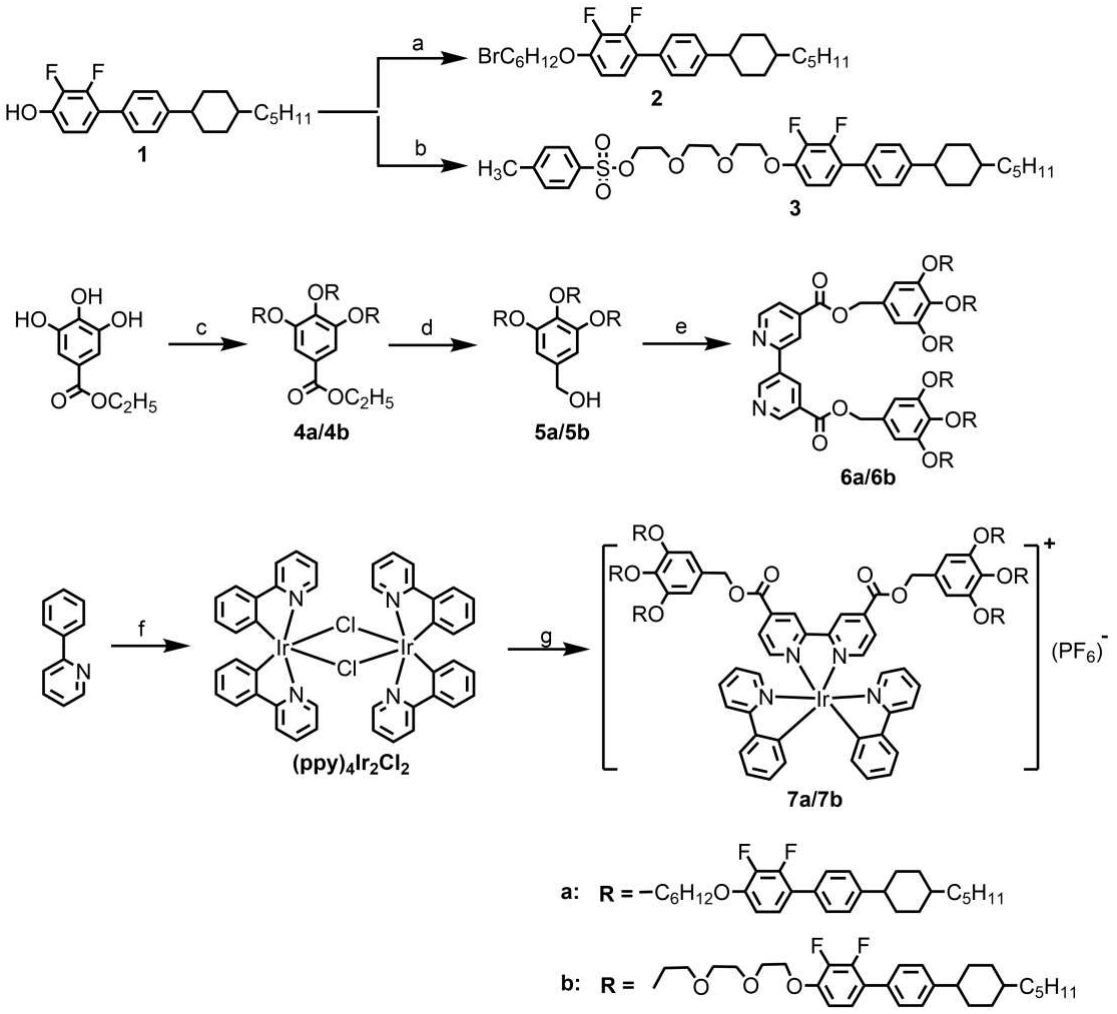

Reaction conditions: (a) 1,6-dibromohexane, K_2CO_3, KI, acetone, reflux, 24 h; (b) 1,2-bis(2-(p-tosyloxy)ethoxy)ethane, K_2CO_3, KI, acetone, reflux, 24 h; (c) **2** or **3**, K_2CO_3, KI, acetone, reflux, 30 h; (d) $LiAlH_4$, dry THF, room temperature, 8 h; (e) 2,2'-bipyridine-4,4'-dicarbonyl dichloride, Et_3N, CH_2Cl_2, reflux, overnight; (f) 2-phenylpyridine, $IrCl_3 \cdot H_2O$, 2-ethoxylethanol/H_2O = 3:1, 100°C, overnight; (g) $(ppy)_4Ir_2Cl_2$, **6a** or **6b**, KPF_6, MeOH/CH_2Cl_2, reflux, overnight.

Scheme 1. Synthetic routes of complexes **7a** and **7b**.

The synthesis of **7a/7b** is depicted in Scheme 1. Compound **1**, **2**, **4a** and **5a** were prepared according to literature procedures.[39,45] Compounds **2** and **3** were obtained via etherification using K_2CO_3 in acetone solution in good yield (60%–80%). The commercially available ethyl 3,4,5-trihydroxybenzoate reacted with intermediate **2** (or **3**) to give compounds **4a/4b** also by an etherification reaction. Subsequently, a reduction of compound **4a/4b** using $LiAlH_4$ in dry THF at room temperature quantitatively afforded compounds **5a/5b**. The bipyridine ligands **6a/6b** were

synthesized via condensation between **5a/5b** and 2,2'-bipyridine-4,4'-dicarbonyl dichloride in dichloromethane in the presence of triethylamine. Finally, the complexation reaction between **6a/6b** and the 2-phenylpyridine-based chloro bridged iridium dimer afforded the target iridium complexes **7a/7b**, which structures were confirmed via ^{1}H and $^{13}C\{^{1}H\}$ NMR spectroscopy, MALDI-MS and elemental analysis (ESI†).

Thermal properties

The thermal properties of the complexes were initially studied by thermogravimetric analysis (TGA, Figure S1), differential scanning calorimetry (DSC, Figure S2) and polarizing optical microscope (POM, Figure S3), and the relevant data are given in Table 1.

Table 1 [a] Thermal properties of complexes 7a and 7b

Complexes	T_d (5%) /ºC	Phase, transition temperature (ΔH J/g)
7a	336	Cr 209 (0.20) Cr_1 216 (0.25) SmA 235 (5.17) I
7b	324	Cr 156 (1.08) SmA 177 (1.41) I

[a] Scan rate: 10 °C min^{-1}. Transition temperatures from the DSC peaks on second heating. Phase nomenclature: Cr, Cr_1 = crystal, S_m = smectic mesophase, I = isotropic liquid.

Before exploring the mesomorphic property of the iridium complexes, TGA measurement was carried out to evaluate their thermal stability. Notably, both complexes show good thermal stability with the decomposition temperature of 336 ºC and 324 ºC for **7a** and **7b** at 5% weight loss, respectively. Then, DSC and POM measurements were carried out to investigate the thermotropic behavior of both iridium complexes. As depicted in Figure S2a, **7a** shows several reversible phase transition peaks on heating and cooling processes in the range of room temperature to 250 ºC,

assigned to crystal-crystal, crystal-liquid crystal and liquid crystal-isotropic liquid state, respectively. For the DSC trace of **7b** (Figure S2b), the transition at 156 ºC is from crystal to mesomorphic phase on the second heating cycle, while it is an isotropic fluid above 180ºC. Correspondingly, two reversible exothermic peaks are also observed upon cooling processes. Compared to **7a**, **7b** possesses clearly decreased both the melting point and clearing point due to the triethylene glycol substituent. According to the DSC results, POM was measured to investigate the mesomorphic behavior. Both iridium complexes present clear birefringence texture upon cooling processing from isotropic phase, a typical characteristic of mesophase (Figure S3). Especially, complex **7b** presented excellent fluidity when it was sheared in the mesomorphic state (Figure S4).

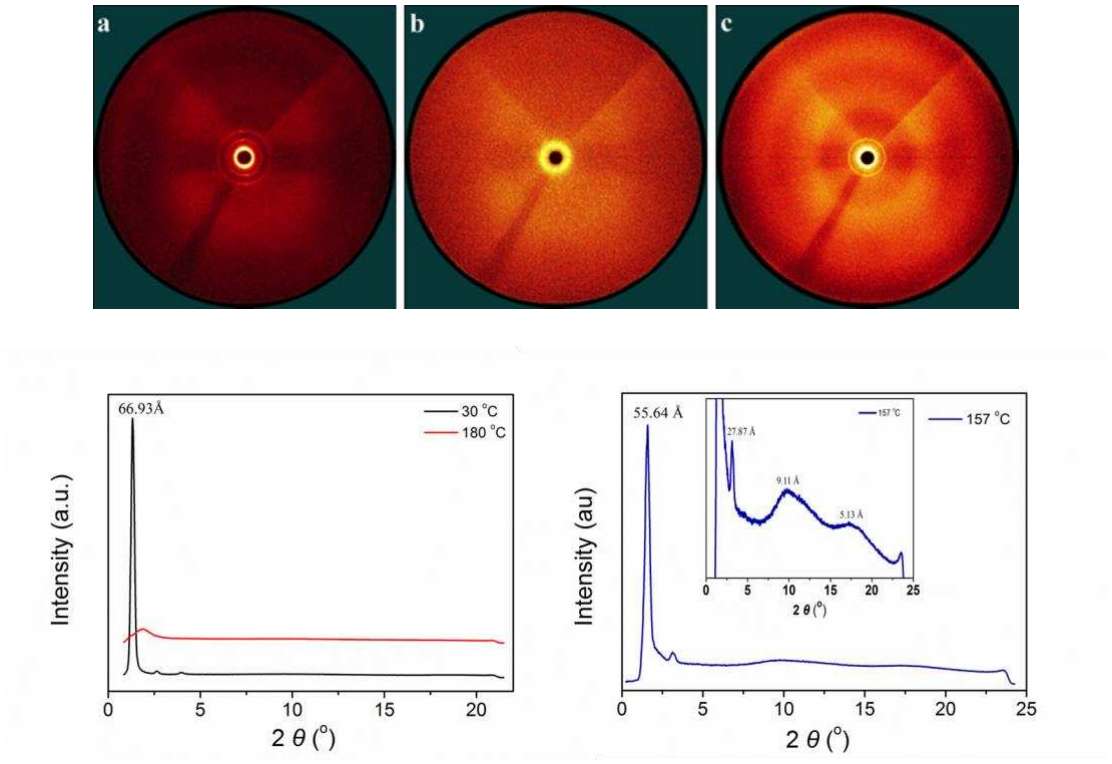

Figure 1. 2DWAXS pattern of **7b** at (a) 30 ºC; (b) 180 ºC; (c) 157 ºC) and the corresponding equatorial integration.

To further confirm the mesomorphic state, taking **7b** as an example, temperature-

dependent X-ray diffraction (XRD) was carried out. As shown in Figure 1, complex **7b** shows an ordered crystal structure at room temperature, which presents a very strong reflection peak with two weak reflection peaks at low angle region. When heating to 180ºC, the XRD pattern displays nothing except a broad scatter peak in small angle region, implying isotropic liquid. Upon cooling from the isotropic liquid (Figure 1c, 157ºC), the XRD pattern for **7b** shows one sharp and intense reflection centered at 2θ = 1.59º (55.6 Å) and a weak reflection at 2θ = 3.17º (27.8 Å). The ratio of their reciprocal *d* spacing is 1:2 and they are indexed as the (001) and (002) reflections of a smectic phase. A broad reflection was observed at 2θ = 9.71º (9.1 Å) was assigned to poorly correlated separation of iridium atoms, as reported previously for neutral iridium complexes.[45] Finally a weaker broad reflection was observed at 2θ = 17.3º (5.1 Å) and attributed to molten alkyl chains and triethyleneglycol chains.

Photophysical properties

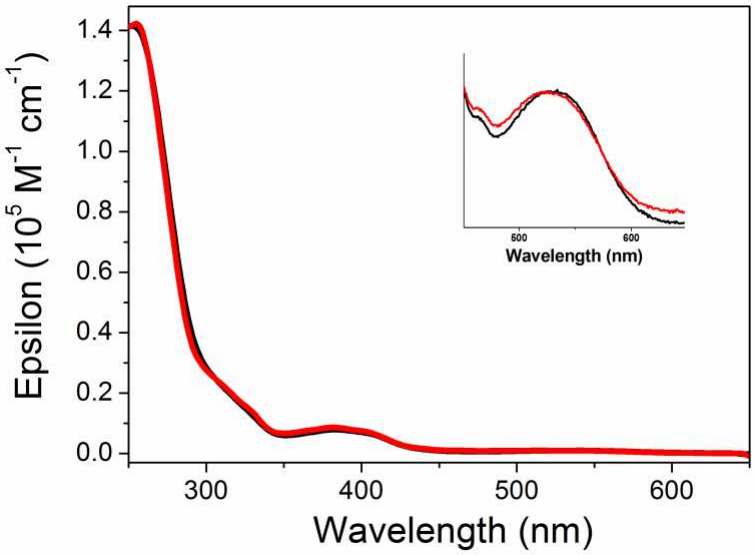

Figure 2. UV-vis spectra of **7a** (black) and **7b** (red) in CH_2Cl_2 at room temperature (10^{-5} M). Inset: zoom into the 500-600 nm region (10^{-4} M).

Table 2 Photophysical characterization of iridium complexes **7a** and **7b**

Compounds	[a]UV-vis /nm	Emission /nm	[d]Φ_{PL}	τ /ns	[g]E^{ox} /V	[h]E_g^{opt} /eV	[i]E_{HOMO} /eV	[j]E_{LUMO} /eV
7a	279, 384, 405, 537	[b]656 [c]640	0.06	[e]80.1 [f]508	0.79	2.21	-5.19	-2.98
7b	279, 384, 404, 529	[b]657 [c]651	0.04	[e]89.3 [f]2320	0.85	2.23	-5.25	-3.02

[a]Measured in CH_2Cl_2 (10^{-5} M) solution at room temperature. [b,e]Excitation wavelength λ = 530 nm, measured in degassed CH_2Cl_2 (10^{-5} M) solution at room temperature. [c]Measured in neat film. [d]Measured in CH_2Cl_2 solution at room temperature using $[Ir(piq)_2(acac)]$ as reference, ref.[46] [f]measured in neat film after degassed. [g]0.1 M $Bu_4N^+PF_6^-$ in CH_2Cl_2 (*vs* NHE) at a scan rate of 100 mV/s. The potential are corrected *vs* SCE. [h]Calculated from the cross point of UV and PL spectra ($E_g = 1240/\lambda_{cross\ point}$). [j]HOMO energy estimated from the following relationship: HOMO (eV) = -4.4 eV – eE^{ox}. [i]LUMO energy estimated from the following relationship: LUMO (eV) = HOMO + E_g.

Both iridium complexes show the same electronic absorption spectra in CH_2Cl_2 (10^{-5} M) at room temperature, Figure 2. Three well-resolved absorption bands between 250 nm and 550 nm are observed. The absorption bands located at about 279 nm with high molar extinction coefficient ($\varepsilon \sim 4.4 \times 10^4\ M^{-1}\ cm^{-1}$) are attributed to spin-allowed ligand π-π* transitions of the ligands and of the biphenyl mesogenic groups. The moderately intense absorption bands in the range of 350-450 nm ($\varepsilon \sim 1.06 \times 10^4\ M^{-1}\ cm^{-1}$) are assigned to mixed metal-to-ligand and ligand-to-ligand (between phenylpyridine and bipyridine ligand) charge-transfer transitions largely of singlet character, while the weak absorption band at about 530 nm ($\varepsilon \sim 10^3\ M^{-1}\ cm^{-1}$) is largely of triplet character.[47]

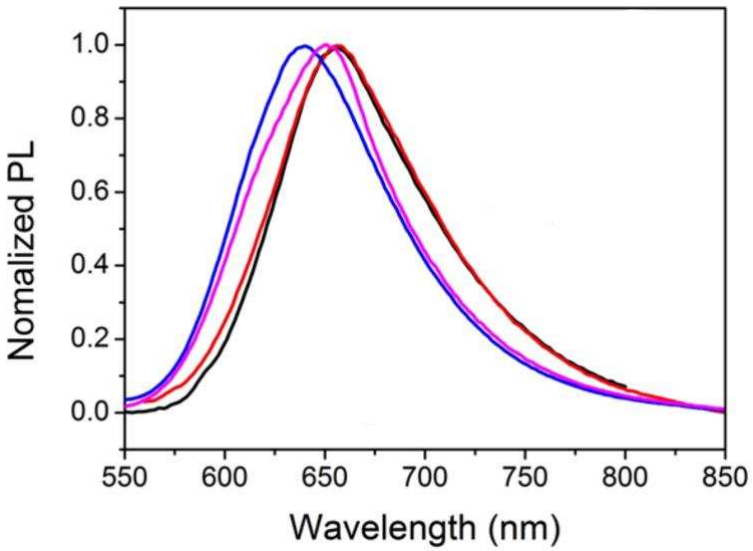

Figure 3. Emission spectra (10^{-5} M) of **7a** (black: in CH_2Cl_2; blue: neat film) and **7b** (red: in CH_2Cl_2; mauve: neat film).

Upon excitation at λ = 530 nm of CH_2Cl_2 solutions, both complexes exhibit red emission with a maximum emission peak at 656 nm (Figure 3). **7a/7b** possess low luminescent quantum yield of 0.04-0.06 and similar emission decay times of 81 and 89 *ns* (Table 2). These values are identical within experimental error and are the same as the parent complex without mesogenic groups, $[Ir(ppy)_2(deeb)][PF_6]$.[47] This demonstrates that the mesogenic groups and the linkers have no significant impact on the photophysical properties of **7a/7b**. Interestingly, the emission of **7a/7b** in neat films is slightly blue shifted (6-16 nm, Figure 3) in contrast to the usual behavior of ionic iridium complexes.[48] This particular effect is attributed to the pendant mesogenic groups that act as a molecular host decreasing interactions between the core complexes. Additionally, complex **7a** showed much brighter emission than that in solution, which is similar with the AIE phosphorescent materials based on both ionic and neutral iridium complexes.[49-51] Therefore, this abnormal phenomenon probably indicates that that these kind of iridium complexes could be AIE-active molecules.

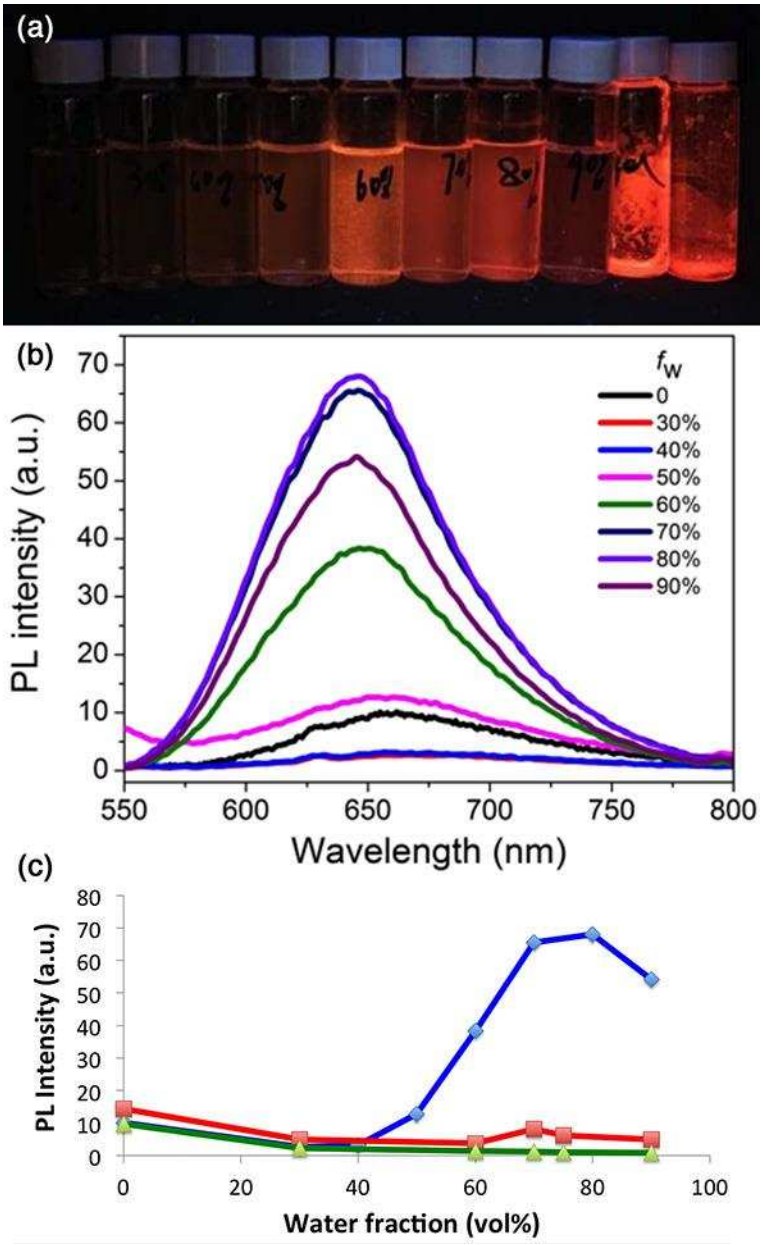

Figure 4. (a) Photograph of **7a** 10^{-5} M in THF-water mixtures with different vol% values (from left to right (f_w): 0 %, 30 %, 40 %, 50 %, 60 %, 70 %, 80 %, 90 % and solid) taken under UV illumination at 365 nm; (b) Emission spectra of **7a** in THF-water mixtures, λ_{ex} = 530 nm; (c) Change in PL intensity of **7a** (blue), **7b** (red) and parent complex $[Ir(ppy)_2(deeb)][PF_6]$ (green).

In order to demonstrate this hypothesis, the luminescence of **7a**/**7b** and their parent complex $[Ir(ppy)_2(deeb)][PF_6]$ were recorded in THF-water mixture with different water fraction (f_w, the concentration of the complex in the mixture kept constant at 10^{-5} M). The PL intensity of **7b** and $[Ir(ppy)_2(deeb)][PF_6]$ decreases as the concentration of water increases (Figure S5 and S6), suggesting that they could not effectively form

the aggregates in the mixture and the increased solvent polarity in THF/H_2O mixture leads to an increase of the rate of non-radiative decay.

As evident from Figure 4, complex **7a** shows weak emission in pure THF, while the emission is almost completely quenched in f_w of 30 %. This phenomenon is attributed to the twisted intramolecular charge-transfer (TICT) effect in the gradually strengthened solvent polarity in THF/water mixture with a higher fraction of polar water.[52] Compared to the emission both in solution and neat film, this TICT effect is assigned to the MLCT emission. As f_w was increased to 60%, the PL intensity is dramatically enhanced concomitant with an obviously blue-shifted emission, which follows the blue shift observed in neat films (Figure 3). The emission intensity present the maximum level at 645 nm as f_w promoted to 80 %, which is about 7-fold higher than the emission intensity in pure THF. This result can be attributed to the aggregate formation due to the decreased solvating ability of the aqueous mixture and the lower impact of the polarity of solvent on complex **7a**. Concomitantly, the rotation of the phenyl rings of mesogenic moiety was greatly restricted in the aggregate state.[52] When f_w was increased to 90 %, a sharply decreased emission is observed, which is attributed, according to previous reports,[53] to the aggregates reaching a large size and sedimenting. In addition, the vivid emission images (Figure 4a and Figure S7) under UV irradiations also directly show the AIE process. The absence of AIE with **7b** is attributed to the higher solubility in water of the triethyleneglycol chains compared to the hexyl linker of **7a**. As a result, aggregation is prevented in **7b** even with the water insoluble mesogenic groups. As the parent complex without mesogenic groups also lacks AIE

property, it demonstrates the importance of these pendent mesogenic groups to obtain AIE, in addition to the crucial choice of the linker.

To show the increased aggregation of iridium complexes in THF-water mixture with increased water content, scanning electron microscopy (SEM) was carried out on samples with f_w of 30% and 90%, as shown in Figure S8. The SEM images display only few small aggregates for the f_w of 30% sample, whereas much larger aggregates are observed in the f_w of 90% mixture. These micrometer sized aggregates can also explain the drop in luminescence at 90% as they would sediment at the bottom of the vial.[53]

Polarized electroluminescence property

To get insight into the polarized EL properties of these metallomesogens, both **7a** and **7b** were used as non-doped emitter in OLEDs. Generally, the linear polarized OLEDs employed an aligned film as the emitter, which plays a critical role to achieve the polarized light. So far, various methodologies have been devoted to achieve the aligned emitting layer. For example, mechanical stretching, friction-transfer technique, Langmuir-Blodgett (LB) technique, liquid-crystal self-organization and rubbing and annealing.[4,54,55] In this contribution, we mainly explored the effect of rubbing and annealing on the polarized emission. The detailed procedures and device configurations are listed in Experimental Section.

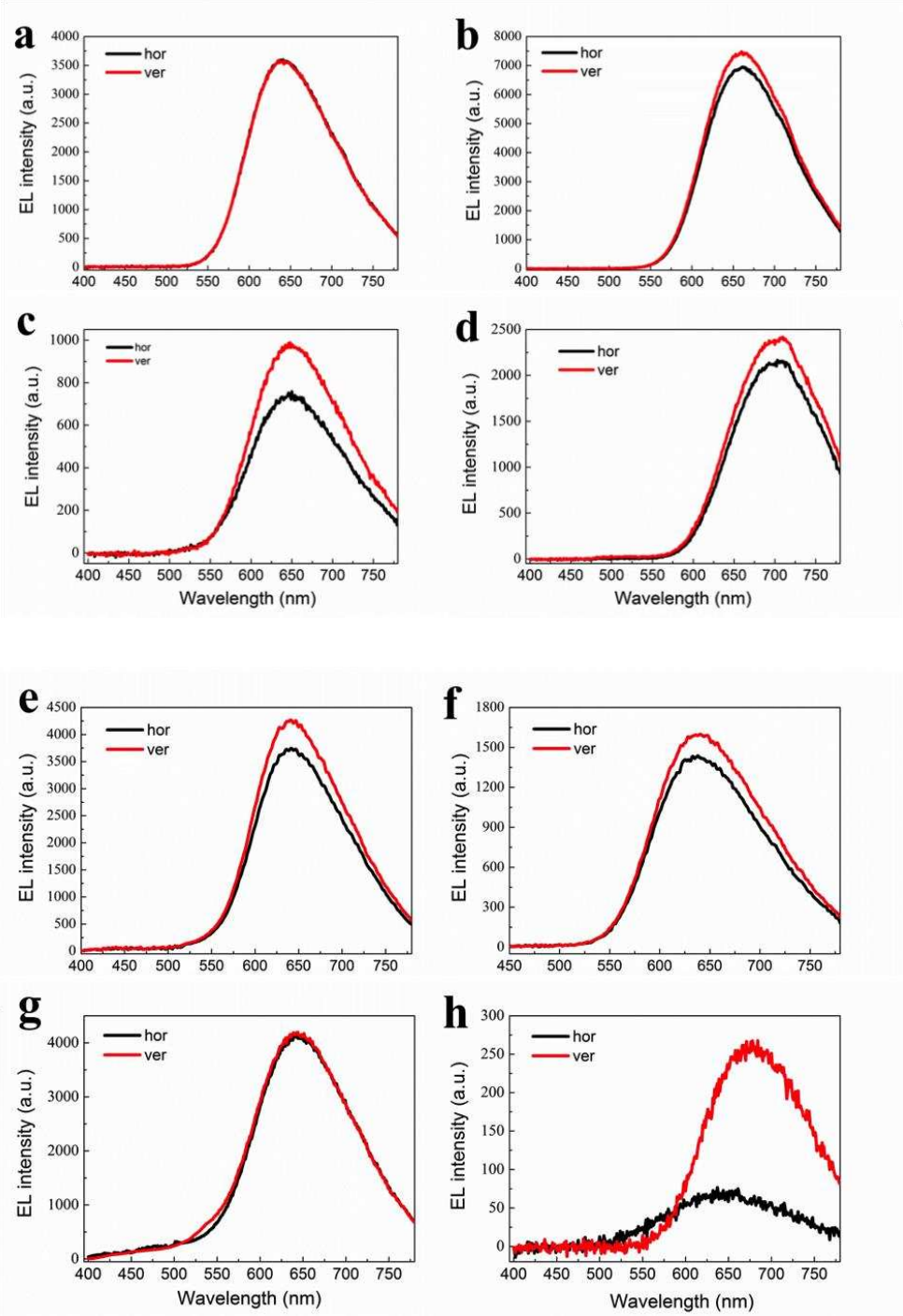

Figure 5 EL spectra from devices I, II, III and IV at 10 mA/cm^2 after a linear polarizer at two orthogonal directions (vertical: parallel to rubbing direction; horizontal: orthogonal to rubbing direction): (a) **7a** in device I; (b) **7a** in device II; (c) **7b** in device I; (d) **7b** in device II; (e) **7a** in device III; (f) **7a** in device IV; (g) **7b** in device III; (h) **7b** in device IV.

Initially, two configurations without and with an electron transporting layer (ETL) were tested: ITO/PEDOT:PSS/PVK/Ir complex/Ca/Al (device I) and

ITO/PEDOT:PSS/PVK/Ir complex/B3PYMPM/Ca/Al (device II). In these cases, the emissive layer was simply spin-coated onto the hole-transporting layer of PVK without receiving any specific treatment and B3PYMPM was deposited as the ETL.

The EL spectra were measured with a polarizer placed at two orthogonal directions, noted horizontal (hor) and vertical (ver) (Figure 5). All the EL spectra showed a red broad emission at about 640 nm but for **7b** in device II, which displayed a red-shifted spectrum peaking at 707 nm,[56] which could be attributed to electroplex emission between**7b** and the ETL because of the different emission of the mixture of complex **7b** and the ETL. For **7a**, no polarization of EL was observed in device I as the two EL spectra, horizontal and vertical, are perfectly superimposed (Figure 5a), while a minor polarized EL was observed in device II (Figure 5b). The EL dichroic ratio (R) is calculated from the relation of $R_{EL} = I_{\parallel}/I_{\perp}$ to be 1.1, where $I_{\parallel}$ and $I_{\perp}$ are the maximum intensities of parallel and perpendicular to the rubbing direction. Conversely, **7b** exhibited polarized EL emission with R of 1.4 and 1.2 in device I and II, respectively. Even so, both the devices performances are dissatisfied, probably due to the very poor carrier transfer property and absent host matrix. As shown in Table S1 (ESI†), device II based on complex **7a**/or **7b** displayed better device performance than that of device I, owing to the additional ETL layer. The device based on complex 7a showed a highest external quantum efficiency (EQE) of 0.85 % in device II.

In an attempt to further improve the dichroic ratio, two approaches were tested to align the emissive layer using the configuration of device II. One approach was to rub the PVK layer, and then the emissive layer was spin-coated onto the rubbed PVK film.

The other approach was to rub the emitting layer directly. The configurations of both devices are therefore ITO/PEDOT:PSS/PVK(rubbed)/Ir complex/B3PYMPM/Ca/Al (device III) and ITO/PEDOT:PSS/PVK/Ir complex(rubbed)/B3PYMPM/Ca/Al (device IV).

The treatments had only little impact for **7a**, as both devices III and IV showed a polarized EL emission with R of only 1.2 and 1.1, respectively (Figure 5e and 5d). Rubbing the PVK layer had even a detrimental effect for **7b** as the EL was not polarized anymore (Figure 5g). In contrast, **7b** in device IV showed a distinctive polarized EL emission with the highest R of 4, which is significantly higher than achieved with other devices. This result demonstrates that a rubbed emissive layer is an effective method for achieving linearly polarized electroluminescence. Notedly, the device IV of **7b** shows relatively weak polarized EL at ca. 635 nm along the horizontal direction, whereas more intense, red-shifted EL (ca. 675 nm) was observed along the vertical direction. This implies that the rubbing could have an effect on the exciplex emission or electroplex emission. On the other side of the coin, rubbing on the emissive layer has an obvious adverse effect on the device performance. Complex **7a** based device III possesses a EQE up to 1.1 % while there is only 0.04 in device IV, may be due to the destroyed emissive layer. Although the efficiency of the OLED devices as well as polarization ratio are very modest to be practically useful, this research demonstrates that cyclometalated iridium complex based luminescent metallomesogens can be used as an emitter in OLEDs.

Conclusions

In summary, two novel phosphorescent, ionic, liquid-crystalline iridium complexes, **7a** and **7b**, have been synthesized and studied. Both complexes showed stable enantiotropic mesophase. The complex containing the triethyleneglycol linker (**7b**) possessed lower melting point and clearing point than the complex with an alkyl chain as the linker (**7a**). Interestingly, **7a** displayed aggregation induced emission properties when water was added to a solution of the complex in THF. Because of the triethyleneglycol linker, **7b** is too soluble in water to form aggregates and remained AIE silent. Delightfully, **7b** gave polarized electroluminescence with a promising polarization ratio of 4 when the emissive layer was mechanically rubbed. However, the devices using the analogue **7a** displayed little to no polarization. This difference of behavior is attributed to the lower melting and clearing points of **7b**, which ease the alignment of the complexes during the rubbing process.

Despite the low luminous efficiencies, which need further improvement, to the best of our knowledge, this prototype is the first example of directly polarized electroluminescence based on phosphorescent iridium complexes. Importantly, this work demonstrates the importance of the linker to obtain phosphorescent metallomesogens with desirable properties and future work aims at developing new materials with finely engineered linkers allowing for both AIE and good polarization ratio in a single complex to improve the performance of the devices.

Acknowledgements

Financial support is acknowledged from the National Natural Science Foundation of China (51773021, U1663229, 51473140), Natural Science Foundation of Hunan Province (2017JJ2245), , European Union (MC-IIF-329199), the Talent project of Jiangsu Specially-Appointed Professor and the University of York and the EPSRC for funds to purchase the SAXS instrument.

References

1 P. Dyreklev, M. Berggren, O. Inganas, M. R. Andersson, O. Wennerstrom and T. Hjertberg, Polarized electroluminescence from an oriented substituted polythiophene in a light-emitting diode. *Adv. Mater.*, 1995, **7**, 43-45.

2 M. Grell and D. D. C. Bradley, Polarized luminescence from oriented molecular materials. *Adv. Mater.*, 1999, **11**, 895-905.

3 M. O'Neill and S. M. Kelly, Liquid crystals for charge transport, luminescence, and photonics. *Adv. Mater.*, 2003, **15**, 1135-1146.

4 Y. Wang, J. Shi, J. Chen, W. Zhu and E. Baranoff, Recent progress in luminescent liquid crystal materials: design, properties and application for linearly polarised emission. *J. Mater. Chem. C*, 2015, **3**, 7993-8005.

5 H. Tokuhisa, M. Era and T. Tsutsui, Polarized electroluminescence from smectic mesophase. *Appl. Phys. Lett.*, 1998, **72**, 2639-2641.

6 Y. H. Geng, A. C. A. Chen, J. J. Ou, S. H. Chen, K. Klubek, K. M. Vaeth and C. W. Tang, Monodisperse glassy-nematic conjugated oligomers with chemically tunable polarized light emission. *Chem. Mater.*, 2003, **15**, 4352-4360.

7 S. W. Culligan, Y. Geng, S. H. Chen, K. Klubek, K. M. Vaeth and C. W. Tang, Strongly polarized and efficient blue organic light-emitting diodes using monodisperse glassy nematic oligo(fluorene)s. *Adv. Mater.*, 2003, **15**, 1176-1180.

8 A. C. A. Chen, S. W. Culligan, Y. Geng, S. H. Chen, K. P. Klubek, K. M. Vaeth and C. W. Tang, Organic polarized light-emitting diodes via förster energy transfer using monodisperse conjugated oligomers. *Adv. Mater.*, 2004, **16**, 783-788.

9 A. Hamidi-Sakr, L. Biniek, S. Fall and M. Brinkmann, Precise control of lamellar thickness in highly oriented regioregular poly(3-Hexylthiophene) thin films prepared by high-temperature rubbing: correlations with optical properties and charge transport. *Adv. Funct. Mater.*, 2016, **26**, 408-420.

10 M. Grell, W. Knoll, D. Lupo, A. Meisel, T. Miteva, D. Neher, H. G. Nothofer, U. Scherf and A. Yasuda, Blue polarized electroluminescence from a liquid crystalline polyfluorene. *Adv. Mater.*, 1999, **11**, 671-675.

11 A. Liedtke, M. O'Neill, A. Wertmoller, S. P. Kitney and S. M. Kelly, White-light OLEDs using liquid crystal polymer networks. *Chem. Mater.*, 2008, **20**, 3579-3586.

12 M. A. Baldo, S. Lamansky, P. E. Burrows, M. E. Thompson and S. R. Forrest, Very high-efficiency green organic light-emitting devices based on electrophosphorescence. *Appl. Phys. Lett.*, **1999**, 75, 4-6.

13 T. Tsutsui, M. J. Yang, M. Yahiro, K. Nakamura, T. Watanabe, T. Tsuji, Y. Fukuda,

T. Wakimoto and S. Miyaguchi, High quantum efficiency in organic light-emitting devices with iridium-complex as a triplet emissive center. *Jpn. J. Appl. Phys.*, 1999, **38**, L1502.

14 J. Kalinowski, V. Fattori, M. Cocchi and J. A. G. Williams, Light-emitting devices based on organometallic platinum complexes as emitters. *Coord. Chem. Rev.*, 2011, **255**, 2401-2425.

15 M. Cocchi, J. Kalinowski, D. Virgili, V. Fattori, S. Develay and J. A. G. Williams, Single-dopant organic white electrophosphorescent diodes with very high efficiency and its reduced current density roll-off. *Appl. Phys. Lett.*, 2007, **90**, 163508-163510.

16 S.-L. Lai, W.-Y. Tong, S. C. F. Kui, M.-Y. Chan, C.-C. Kwok and C.-M. Che, High Efficiency white organic light-emitting devices incorporating yellow phosphorescent platinum(II) complex and composite blue host. *Adv. Funct. Mater.*, 2013, **23**, 5168-5176.

17 K. Y. Liao, C. W. Hsu, Y. Chi, M. K. Hsu, S. W. Wu, C. H. Chang, S. H. Liu, G. H. Lee, P. T. Chou, Y. Hu and N. Robertson, Pt(II) metal complexes tailored with a newly designed spiro-arranged tetradentate ligand; harnessing of charge-transfer phosphorescence and fabrication of sky blue and white OLEDs. *Inorg. Chem*., 2015, **54**, 4029-4038.

18 T. Fleetham, G. Li and J. Li, Efficient red-emitting platinum complex with long operational stability. *ACS Appl. Mater. Interfaces*, 2015, **7**, 16240-16246.

19 X.; Xu, X. Yang, J. Zhao, J. S. Dang, Z. Huang, X. Yan, G. Zhou and D. Wang, Phosphorescent platinum(II) complexes bearing 2-vinylpyridine-type ligands: synthesis, electrochemical and photophysical properties, and tuning of electrophosphorescent behavior by main-group moieties. *Inorg. Chem.*, 2014, **53**, 12986-13000.

20 A. Poloek, C.-W. Lin, C.-T. Chen and C.-T. Chen, High colour rendering index and colour stable hybrid white efficient OLEDs with a double emitting layer structure using a single phosphorescence dopant of heteroleptic platinum complexes. *J. Mater. Chem. C*, 2014, **2**, 10343-10356.

21 G. Li, T. Fleetham and J. Li, Efficient and stable white organic light-emitting diodes employing a single emitter. *Adv*. *Mater*., 2014, **26**, 2931-2936.

22 K. Li, G. Cheng, C. Ma, X. Guan, W.-M. Kwok, Y. Chen, W. Lu and C.-M. Che, Light-emitting platinum(ii) complexes supported by tetradentate dianionic bis(N-

heterocyclic carbene) ligands: towards robust blue electrophosphors. *Chemical Science*, 2013, **4**, 2630-2644.

23 L.-M. Huang, G.-M. Tu, Y. Chi, W.-Y. Hung, Y.-C. Song, M.-R. Tseng, P.-T. Chou, G.-H. Lee, K.-T. Wong, S.-H. Cheng and W.-S. Tsai, Mechanoluminescent and efficient white OLEDs for Pt(II) phosphors bearing spatially encumbered pyridinyl pyrazolate chelates. *J. Mater. Chem. C*, 2013, **1**, 7582-7592.

24 C. Damm, G. Israel, T. Hegmann and C. Tschierske, Luminescence and photoconductivity in mononuclear ortho-platinated metallomesogens. *J. Mater. Chem.*, 2006, **16**, 1808-1816.

25 T. Hegmann, J. Kain, S. Diele, B. Schubert, H. Bögel and C. Tschierske, Molecular design at the calamitic/discotic cross-over point. Mononuclear ortho-metallated mesogens based on the combination of rod-like phenylpyrimidines and -pyridines with bent or half-disc-shaped diketonates. *J. Mater. Chem.*, 2003, **13**, 991-1003.

26 V. N. Kozhevnikov, B. Donnio and D. W. Bruce, Phosphorescent, terdentate, liquid-crystalline complexes of platinum(II): stimulus-dependent emission. *Angew. Chem. Int. Ed.,* 2008, **47**, 6286-6289.

27 M. Krikorian, S. Liu and T. M. Swager, Columnar liquid crystallinity and mechanochromism in cationic platinum(II) complexes. *J. Am. Chem. Soc.*, 2014, **136**, 2952-2955.

28 C. T. Liao, H. H. Chen, H. F. Hsu, A. Poloek, H. H. Yeh, Y. Chi, K. W. Wang, C. H. Lai, G. H. Lee, C. W. Shih and P. T. Chou, Mesomorphism and luminescence properties of platinum(II) complexes with tris(alkoxy)phenyl-functionalized pyridyl pyrazolate chelates. *Chemistry*, 2011, **17**, 546-556.

29 A. Santoro, A. C. Whitwood, J. A. G. Williams, V. N. Kozhevnikov and D. W. Bruce, Synthesis, Mesomorphism, and Luminescent Properties of Calamitic 2-Phenylpyridines and Their Complexes with Platinum(II). *Chem. Mater.*, 2009, **21**, 3871-3882.

30 T. Sato, H. Awano, O. Haba, H. Katagiri, Y. J. Pu, T. Takahashi and K. Yonetake, Synthesis, characterization, and polarized luminescence properties of platinum(II) complexes having a rod-like ligand. *Dalton Trans.*, 2012, **41**, 8379-8389.

31 M. Spencer, A. Santoro, G. R. Freeman, A. Diez, P. R. Murray, J. Torroba, A. C. Whitwood, L. J. Yellowlees, J. A. Williams and D. W. Bruce, Phosphorescent, liquid-crystalline complexes of platinum(II): influence of the beta-diketonate co-ligand on mesomorphism and emission properties. *Dalton Trans.*, 2012, **41**,

14244-14256.

32 Y. Wang, Y. Liu, J. Luo, H. Qi, X. Li, M. Nin, M. Liu, D. Shi, W. Zhu and Y. Cao, Metallomesogens based on platinum(II) complexes: synthesis, luminescence and polarized emission. *Dalton Trans.*, 2011, **40**, 5046-5051.

33 S.-H. Liu, M.-S. Lin, L.-Y. Chen, Y.-H. Hong, C.-H. Tsai, C.-C. Wu, A. Poloek, Y. Chi, C.-A. Chen and S. H. Chen, Polarized phosphorescent organic light-emitting devices adopting mesogenic host–guest systems. *Org. Electron.*, 2011, **12**, 15-21.

34 Y.-T. Tsai, C.-Y. Chen, L.-Y. Chen, S.-H. Liu, C.-C. Wu, Y. Chi, S. H. Chen, H.-F. Hsu and J.-J. Lee, Analyzing nanostructures in mesogenic host–guest systems for polarized phosphorescence. *Org. Electron.*, 2014, **15**, 311-321.

35 M. Zhu, J. Zou, X. He, C. Yang, H. Wu, C. Zhong, J. Qin and Y. Cao, Triphenylamine dendronized iridium(III) complexes: robust synthesis, highly efficient nondoped orange electrophosphorescence and the structure–property relationship. *Chem. Mater.*, 2012, **24**, 174-180.

36 W. Zhu, Y. Mo, M. Yuan, W. Yang and Y. Cao, Highly efficient electrophosphorescent devices based on conjugated polymers doped with iridium complexes. *Appl. Phys. Lett*., 2002, **80**, 2045-2047.

37 W. Z. Yuan, Z.-Q. Yu, P. Lu, C. Deng, J. W. Y. Lam, Z. Wang, E.-Q. Chen, Y. Ma and B. Z. Tang, High efficiency luminescent liquid crystal: aggregation-induced emission strategy and biaxially oriented mesomorphic structure. *J. Mater. Chem.*, 2012, **22**, 3323-3326.

38 M. Mitani, S. Ogata, S. Yamane, M. Yoshio, M. Hasegawa and T. Kato, Mechanoresponsive liquid crystals exhibiting reversible luminescent color changes at ambient temperature. *J. Mater. Chem. C*, 2016, **4**, 2752-2760.

39 E. D. Baranoff, J. Voignier, T. Yasuda, V. Heitz, J.-P. Sauvage and T. Kato, A liquid-crystalline [2]catenane and its copper(I) complex. *Angew. Chem. Int. Ed.*, 2007, **46**, 4680-4683.

40 X. Zhang, C.-H. Hsu, X. Ren, Y. Gu, B. Song, H.-J. Sun, S. Yang, E. Chen, Y. Tu, X. Li, X. Yang, Y. Li and X. Zhu, Supramolecular [60]Fullerene liquid crystals formed by self-organized two-dimensional crystals. *Angew. Chem. Int. Ed.*, 2015, **54**, 114-117.

41 Y. Molard, F. Dorson, V. Cîrcu, T. Roisnel, F. Artzner and S. Cordier, Clustomesogens: liquid crystal materials containing transition-metal clusters. *Angew. Chem. Int. Ed.*, 2010, **49**, 3351-3355.

42 E. I. Szerb, A. M. Talarico, I. Aiello, A. Crispini, N. Godbert, D. Pucci, T. Pugliese and M. Ghedini, Red to Green Switch Driven by Order in an Ionic IrIII Liquid-Crystalline Complex. *Eur. J. Inorg. Chem.*, 2010, **21**, 3270-3277.

43 A. Santoro, A. M. Prokhorov, V. N. Kozhevnikov, A. C. Whitwood, B. Donnio, J. A. Williams and D. W. Bruce, Emissive metallomesogens based on 2-phenylpyridine complexes of iridium(III). *J. Am. Chem. Soc.*, 2011, **133**, 5248-5251.

44 A. M. Prokhorov, A. Santoro, J. A. Williams, D. W. Bruce, Phosphorescent mesomorphic dyads based on tetraacetylethane complexes of iridium(III). *Angew. Chem. Int. Ed.*, 2012, **51**, 95-98.

45 Y. Wang, C. P. Cabry, M. Xiao, L. Male, S. J. Cowling, D. W. Bruce, J. Shi, W. Zhu and E. Baranoff, Blue and green phosphorescent liquid-crystalline iridium complexes with high hole mobility. *Chemistry Eur. J.*, 2016, **22**, 1618-1621.

46 H. A. Bronstein, C. E. Finlayson, K. R. Kirov, R. H. Friend and C. K. Williams, Investigation into the phosphorescence of a series of regioisomeric iridium(III) complexes. *Organometallics*, 2008, **27**, 2980-2989.

47 D. N. Chirdon, C. E. McCusker, F. N. Castellano and S. Bernhard, Tracking of tuning effects in bis-cyclometalated iridium complexes: a combined time resolved infrared spectroscopy, electrochemical, and computational study. *Inorg. Chem.*, 2013, **52**, 8795-8804.

48 H. J. Bolink, L. Cappelli, S. Cheylan, E. Coronado, R. D. Costa, N. Lardiés, M. K. Nazeeruddin and E. Ortí, Origin of the large spectral shift in electroluminescence in a blue light emitting cationic iridium(iii) complex. *J. Mater. Chem.*, 2007, **17**, 5032-5041.

49 P. Li, Q.-Y. Zeng, H.-Z. Sun, M. Akhtar, G.-G. Shan, X.-G. Hou, F.-S. Li and Z.-M. Su, Aggregation-induced emission (AIE) active iridium complexes toward highly efficient single-layer non-doped electroluminescent devices. *J. Mater. Chem.C*, 2016, **4**, 10464-10470.

50 P. Alam, S. Dash, C. Climent, G. Kaur, A. R. Choudhury, D. Casanova, P. Alemany, R. Chowdhury and I. R. Laskar, ‘Aggregation induced emission’ active iridium(III) complexes with applications in mitochondrial staining. *RSC Adv.*, 2017, **7**, 5642-5648.

51 C. Jin, J. Liu, Y. Chen, R. Guan, C. Ouyang, Y. Zhu, L. Ji and H. Cao, Cyclometalated iridium(III) complexes as AIE phosphorescent probes for real-time

monitoring of mitophagy in living cells. Scientific Report, 2016, 6, 22039-22051.

52 M. Chen, H. Nie, B. Song, L. Li, J. Z. Sun, A. Chen and B. Z. Tang, Triphenylamine-functionalized tetraphenylpyrazine: facile preparation and multifaceted functionalities. *J. Mater. Chem. C*, 2016, **4**, 2901-2908.

53 T. Butler, W. A. Morris, J. Samonina-Kosicka and C. L. Fraser, Mechanochromic luminescence and aggregation induced emission for a metal-free β-diketone. *Chem. Commun.*, 2015, **51**, 3359-3362.

54 S. I. Jo, Y. Kim, J.-H. Baek, C.-J. Yu and J.-H. Kim, Highly polarized emission of the liquid crystalline conjugated polymer by controlling the surface anchoring energy. *Japanese Journal of Applied Physics* 2014, **53**, 03CD04-1-03CD04-4.

55 M. Grell and D. D. C. Bradley, Polarized luminescence from oriented molecular materials. *Adv. Mater.*, 1999, **11**, 895-905.

56 E. Margapoti, V. Shukla, A. Valore, A. Sharma, C. Dragonetti, C. C. Kitts, D. Roberto, M. Murgia, R. Ugo and M. Muccini, Excimer emission in single layer electroluminescent devices based on [ir(4,5-diphenyl-2-methylthiazolo)$_2$(5-methyl-1,10-phenanthroline)]$^+$ [PF6]$^-$, *J. Phys. Chem. C*, 2009, **113**, 12517-12522.

Table of Contents (TOC) Graphic

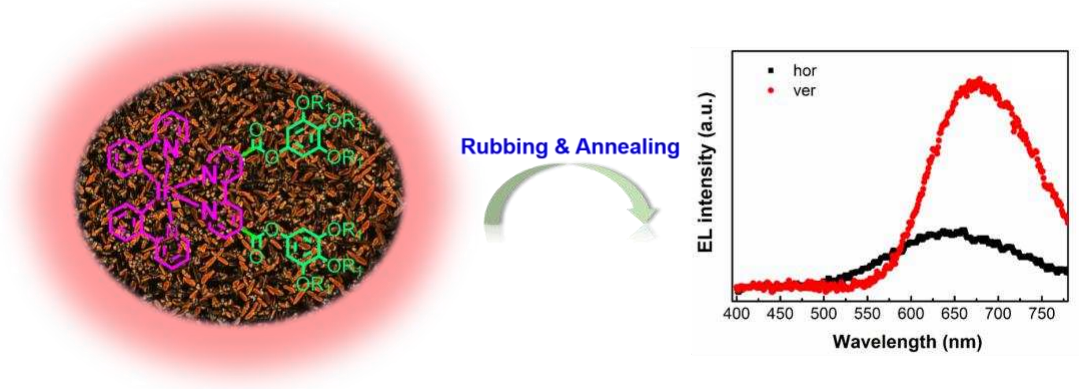

Clearly polarized electroluminescence was obtained from Ionic iridium complex-based metallomesogens.